

# Robust finite element model updating of a large-scale benchmark building structure

E. Matta\* and A. De Stefano

*Department of Structural and Geotechnical Engineering, Politecnico di Torino, Italy*

*(Received September 3, 2011, Revised June 5, 2012, Accepted July 9, 2012)*

**Abstract.** Accurate finite element (FE) models are needed in many applications of Civil Engineering such as health monitoring, damage detection, structural control, structural evaluation and assessment. Model accuracy depends on both the model structure (the form of the equations) and the model parameters (the coefficients of the equations), and can be generally improved through that process of experimental reconciliation known as model updating. However, modelling errors, including (i) errors in the model structure and (ii) errors in parameters excluded from adjustment, may bias the solution, leading to an updated model which replicates measurements but lacks physical meaning. In this paper, an application of ambient-vibration-based model updating to a large-scale benchmark prototype of a building structure is reported in which both types of error are met. The error in the model structure, originating from unmodelled secondary structural elements unexpectedly working as resonant appendages, is faced through a reduction of the experimental modal model. The error in the model parameters, due to the inevitable constraints imposed on parameters to avoid ill-conditioning and under-determinacy, is faced through a multi-model parameterization approach consisting in the generation and solution of a multitude of models, each characterized by a different set of updating parameters. Results show that modelling errors may significantly impair updating even in the case of seemingly simple systems and that multi-model reasoning, supported by physical insight, may effectively improve the accuracy and robustness of calibration.

**Keywords:** model updating; modelling errors; multi-model parameterization; ambient vibration; secondary structural elements; resonant appendages

---

## 1. Introduction

Accurate finite element (FE) models are needed in many applications of Civil Engineering, ranging from health monitoring to structural control, from damage detection to structural evaluation and assessment. FE models used for design may not truly reproduce all the peculiar physical aspects of a real structure and are typically inadequate to replicate the results of experimental testing. FE model updating is the inverse problem of identifying and correcting invalid assumptions in an FE model by matching predicted and observed response. Model updating methods in structural dynamics have been developed and improved for more than 30 years. Extensive reviews of existing techniques can be found in (Friswell and Mottershead 1995, Maia and Silva 1997). The interest in

---

\*Corresponding author, Research Scholar, E-mail: [emiliano.matta@polito.it](mailto:emiliano.matta@polito.it)

this area is proven by the large number of papers recently published on this topic (Aoki and Sabia 2005, McFarland and Mahadevan 2008, Cheung and Beck 2009, Govers and Link 2010, Yan *et al.* 2010, Zapico-Valle *et al.* 2010, Altunişik *et al.* 2010, Bayraktar *et al.* 2010, Yu and Chung 2012). Model updating methods can be mainly grouped into two categories: the non-iterative methods, which are one-step procedures that directly update the elements of the stiffness and mass matrices, and the iterative methods, which are multiple-step procedures that progressively adjust model parameters to match measured data. Non-iterative methods are seldom used in practice since in general they do not preserve the structural connectivity and the physical significance of the model. In iterative methods, model-updating is posed as an optimization problem, in which discrepancies between analytical and experimental results (the residuals) are set as an objective function to be minimized by making changes to a pre-selected set of physical parameters. Because such objective function is generally nonlinear in the parameters, an iterative process is performed, using either gradient-based methods, i.e., sensitivity-based approaches (Li and Law 2010), or direct-search methods, such as simulated annealing, genetic algorithms, hybrid approaches (Levin and Lieven 1998, Jung and Kim 2009).

The success of FE model updating depends on a number of aspects, including having an appropriate numerical model, performing an accurate identification of the experimental modal parameters, choosing a meaningful objective function and using an effective optimization algorithm. Modelling errors, in particular, play a major role in the calibration process. In the presence of modelling errors, an incorrect or shifted baseline model might be reconciled to the measured data, leading to an updated model which would replicate measurements though lacking physical meaning (Saitta *et al.* 2005). Major contributions to modelling error in an FE model are the existence of unmodelled structural members, uncertainty in material properties and geometric section properties of known parameters, incomplete information about boundary conditions and internal connections, nonlinear structural response, energy loss and environmental variability (Sanayei *et al.* 2001). For the sake of convenience, modelling errors may be distinguished into errors in the *model structure* (the form of the equations) and errors in the *model parameters* (the coefficients of the equations) (Mottershead *et al.* 2011). Errors in the model structure depend on wrong assumptions mainly concerning mathematical modelling (differential equations, boundary conditions) and discretisation (meshing, FE type). Every effort should be made to eliminate these errors from the initial FE model, prior to updating. This can be rarely achieved without the application of considerable physical insight. Exploring and comparing several alternative candidates of model structures is a possible way to reduce the impact of this type of error (Robert-Nicoud *et al.* 2005). On the other hand, errors in the model parameters depend on wrong values assigned to the geometrical and mechanical properties of the model (e.g., Young modulus, flexural inertias etc). Once the model structure is determined, removing errors in the parameters is the main objective of model calibration. Usually, however, only few parameters can be simultaneously adjusted, due to the limited amount of data and to computational reasons. Various parameterization techniques exist to make the overall number of *model parameters* depend on a restricted set of *updating parameters*, the latter becoming the variables of the optimization process (Kim and Park 2008, Perera and Ruiz 2008, Adhikari and Friswell 2010, Mthembu *et al.* 2011). The constraint implicit in such dependence constitutes the part of the error in the model parameters which can not be corrected through the updating process.

The present paper reports an application of ambient-vibration-based direct-search model updating to a large-scale benchmark prototype of a building structure in which errors in the model structure

as well as errors in model parameters have been encountered.

Errors in the model structure, on the one hand, originate from the presence of unmodelled secondary structural elements which accidentally happen to work as resonant appendages for the main frame, thus completely altering one of its vibration modes. To the authors' knowledge, such a fortuitous dynamic interaction has never been observed before in buildings. No effort will be done herein to correct the original structure of the baseline FE model. Instead, after providing a consistent physical explanation of the observed phenomenon of dynamic interaction, a mere reduction of the experimental modal model will be performed by removing the altered mode from modal data before calibration.

Errors in the model parameters, on the other hand, originate from the inevitable constraints imposed on parameters to avoid ill-conditioning and under-determinacy. Aiming at exploring the trade-off between the need to limit the updating set for conditioning and computational reasons and the desire to enlarge it as much as possible in order to correct erroneous assumptions, a multi-model parameterization approach is adopted consisting in the generation and solution of a multitude of models, all sharing the same model structure but differing from each other in terms of the updating set. By progressively increasing the number of parameters until reaching non-uniqueness of the solution, and tracking the evolution of the updated model (both in the domain of the search variables and in terms of the objective function), the said trade-off is fathomed and significant information is obtained about the reliability of the calibration process.

The paper is organized as follows. Section 2 will present the benchmark prototype and its testing. Section 3 will describe the FE baseline model. Section 4 will identify the experimental modal model, focusing on the anomalous contribution of secondary structural elements. Section 5 will introduce the multi-model methodology and will use it to update the FE model. Section 6 will draw conclusions.

## **2. The experimental model**

The test structure is a large-scale (2:3) model of a two-storey steel frame building with composite steel-concrete floors (Fig. 1). Built at the Structural Laboratory of the University of Basilicata (Italy), it served as a benchmark for the experimental assessment of the seismic effectiveness of different passive and semi-active control strategies, in the framework of the inter-university Italian DPC-ReLUIIS 2005-08 Project.

The steel structure, consisting of columns and beams orthogonally interconnected into a regular (doubly-symmetrical) three-dimensional frame with one bay in both directions and two rectangular floors (level 1 and 2), is mounted on a rigid horizontal base (level 0), resting on two sliding guides and connected to a dynamic hydraulic actuator which can impart the desired mono-dimensional excitation to the structure. Four equal columns, fixed to the base, extend continuously to the top floor. Eight lateral beams, welded to the columns, support the two composite floors, made up of concrete slabs cast on coffer profiled steel sheeting. The columns free length is 4.00 m, divided into two 2.00m inter-storey heights. The beams length is 4.00 m in the along-excitation (longitudinal or  $x$ -) direction and 3.00 m in the across-excitation (transverse or  $y$ -) direction. The floors thickness is larger than expected because of the sagging effect occurred during concrete casting. In order to house the dissipating devices during tests on the controlled structure, four V-inverted braces, crowned with gusset plates, are bolted at both storeys, parallel to the  $x$ -direction. Columns, beams



Fig. 1 The structural prototype: (a) overall view, (b) beam-column joint, (c) gusset plates atop V-inverted braces, (d) rigid steel base

and braces have I-type cross sections of, respectively, HE140B, IPE180 and HE100A classes, according to the commercial Italian Standard.

At the initial stage of the Project, the need of an accurate numerical model of the benchmark building, for the purposes of test design and results interpretation, motivated a preliminary campaign of dynamic tests on the uncontrolled structure (i.e., with no dissipative device installed). In order to increase the amount of data available so as to improve the numerical conditioning and identify both stiffness and mass properties simultaneously, the classical approach of “perturbed boundary condition testing” (Nalitolela *et al.* 1992) was followed, consisting in perturbing both the structure and, subsequently, the analytical model by adding the same amount of mass at given positions. A total of eight additional lumped masses, consisting of concrete blocks (about 340 kg each), were fixed onto the floors during testing according to three different configurations. Starting from the basic configuration (referred to as BC in the following), characterized by no additional mass, a second doubly-symmetric configuration (SC) was obtained by the addition of four blocks on each storey, then a non-symmetric configuration (NC) was obtained by removing two blocks from the SC configuration at each storey.

For each of the three mass configurations, long-duration vibration tests (2400 s) were conducted

on the uncontrolled structure, using the external excitation furnished by the ambient noise and keeping the sliding guides locked. The dynamic response was measured in terms of acceleration data, recorded at a sampling frequency of 200 Hz. The instrumentation setup consisted of 15 uni-axial high-sensitivity force balance Columbia SA107LN accelerometers (operating in the range  $\pm 0.1$  g), deployed in the most significant observation points: a subset of two accelerometers was placed at the ground level; three subsets of four accelerometers each were mounted in orthogonal pairs at the two opposite corners of, respectively, the base, the first and the second levels; and a single accelerometer was placed on the gusset plate atop one of the two lower braces.

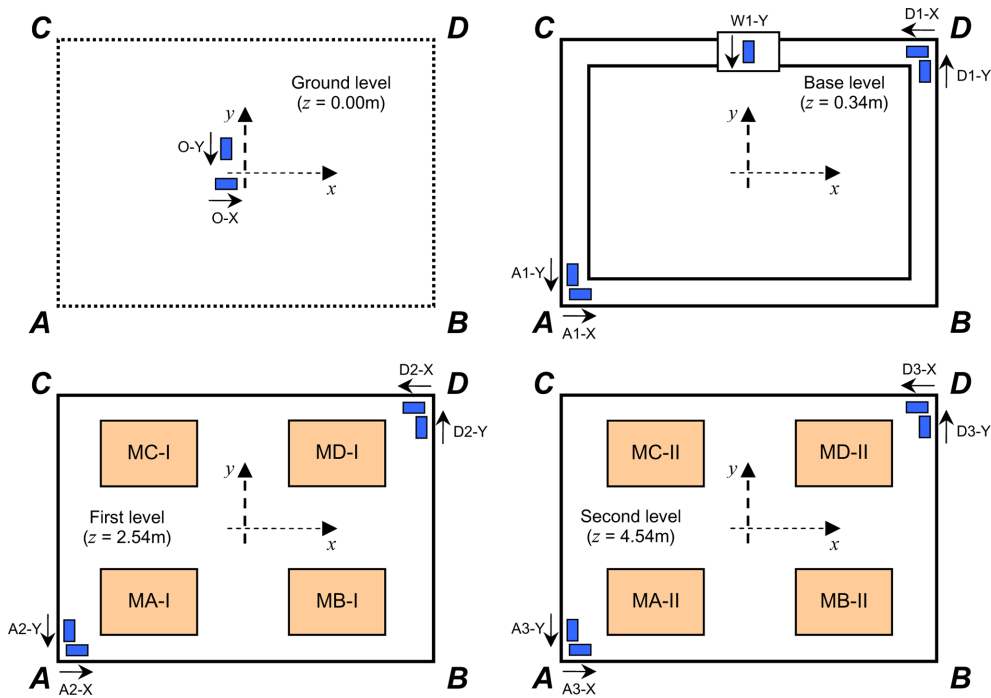


Fig. 2 Location of the accelerometers and of the additional lumped masses

Table 1 Location and properties of the additional lumped masses

Block	Level	Mass (kg)	$e_x$ (m)	$e_y$ (m)	BC	NC	SC
MA-I	1	338	-0.95	-1.00	No	Yes	Yes
MB-I	1	340	0.95	-1.00	No	Yes	Yes
MC-I	1	336	-0.95	1.00	No	No	Yes
MD-I	1	336	0.95	1.00	No	No	Yes
MA-II	2	336	-0.95	-1.00	No	Yes	Yes
MB-II	2	340	0.95	-1.00	No	Yes	Yes
MC-II	2	338	-0.95	1.00	No	No	Yes
MD-II	2	330	0.95	1.00	No	No	Yes

The location of the accelerometers and of the additional masses is described in Fig. 2. Further data, including the position and the inertial properties of concrete blocks, are reported in Table 1.

### 3. The baseline analytical model

The initial (baseline or nominal) analytical model of the test structure is developed on the basis of the original design drawings and in-site visual inspection.

#### 3.1 The model structure

In view of the seeming plainness of the structural prototype, the *model structure* is kept as simple as possible. Due to the low intensity of recorded ambient vibrations a linear dynamic model is assumed. Vertical inextensibility of columns, in-plan rigidity of floors, lumped-mass formulation for columns and beams are assumed as reasonable idealizations, in order to reduce model dimensions without compromising its accuracy. With the same purpose (but with the unexpected effect of severely distorting the model structure, as explained later in Section 4), the dynamics of V-inverted braces is neglected and their mass is conglobed into that of the supporting floor. Other assumptions, which might sound less physically plausible, are however accepted because reconcilable through the subsequent parameter adjustment: columns and beams are modelled as mutually clamped, columns as clamped at their base (as if the base level were perfectly rigid), beams and floor slabs as flexurally independent (as if no mutual connection existed).

Under the said assumptions, the analytical FE *spatial model* is formulated as a three-dimensional 6-degrees-of-freedom (6-DOF) parametric discrete model, whose six coordinates, ordered in the vector  $\boldsymbol{\eta} = \{\delta_{x1} \ \delta_{y1} \ \delta_{\theta1} \ \delta_{x2} \ \delta_{x2} \ \delta_{\theta2}\}^T$ , include the three barycentric components of the in-plan rigid motion of each floor. This spatial model is essentially described by a  $6 \times 6$  mass matrix  $\mathbf{M}$  and by a  $6 \times 6$  stiffness matrix  $\mathbf{K}$ . Damping is not accounted for since of scarce interest in the present case, and anyway low enough to make acceptable the assumption of non-complex modes. Starting from the said analytical *spatial model*, the analytical *modal model* is obtained by solving the eigenvalue problem for the  $\mathbf{M}^{-1}\mathbf{K}$  matrix. It results in the  $6 \times 1$  eigen-frequency vector  $\mathbf{f}$  and in the  $6 \times 6$  eigen-mode matrix  $\Phi$ , whose  $i$ -th column  $\phi_i$  represents the  $i$ -th modal shape, further normalized so as to have unit norm (i.e., unit Euclidean length).

#### 3.2 The model parameters

In the baseline analytical model (including both spatial and modal model), the geometrical and material properties of the structural members are equalled to their expected nominal value. The baseline analytical models corresponding to the three mass configurations, respectively denoted as  $\mathcal{M}_0^{BC}$ ,  $\mathcal{M}_0^{NC}$ ,  $\mathcal{M}_0^{SC}$ , possess the same  $\mathbf{K}$  matrix and different  $\mathbf{M}$ ,  $\mathbf{f}$  and  $\Phi$  matrices. Since they share the same model parameters except the additional masses (which are known data), these three models can be more conveniently regarded as three different states of a unique perturbed baseline model, denoted as  $\mathcal{M}_0$ , and in fact described by a total of one  $\mathbf{K}$  and three triplets of  $\mathbf{M}$ ,  $\mathbf{f}$  and  $\Phi$ . A list of the main nominal parameters assigned to  $\mathcal{M}_0$  is given in Table 2. An axonometric view of the baseline model in the BC configuration is given in Fig. 3, together with a planar schematic view of its six mode-shapes.

Table 2 Nominal parameters of the baseline analytical model  $\mathcal{M}_0$ 

Symbol	Description	Value	Unit
$l_x$	Distance between columns along $x$	4.00	m
$l_y$	Distance between columns along $y$	3.00	m
$h$	Inter-storey height	2.00	m
$E$	Steel Young's modulus	206	GPa
$\rho_s$	Steel mass density	7850	kg/m <sup>3</sup>
$\rho_c$	Composite slab mass density	2500	kg/m <sup>3</sup>
$m_i$	Slab mass at the $i$ -th level ( $i = 1, 2$ )	3539	kg
$J_{oi}$	Slab polar inertia ( $i = 1, 2$ )	7702	kg·m <sup>2</sup>
$I_{cxi}$	Columns bending inertia along $x$ ( $i = 1, 2$ )	$1.509 \cdot 10^{-5}$	m <sup>4</sup>
$I_{cyi}$	Columns bending inertia along $y$ ( $i = 1, 2$ )	$0.550 \cdot 10^{-5}$	m <sup>4</sup>
$I_{bxi}$	$x$ -oriented beams bending inertia ( $i = 1, 2$ )	$1.317 \cdot 10^{-5}$	m <sup>4</sup>
$I_{byi}$	$y$ -oriented beams bending inertia ( $i = 1, 2$ )	$1.317 \cdot 10^{-5}$	m <sup>4</sup>
$I_{ct}$	Columns torsional inertia	$2.000 \cdot 10^{-7}$	m <sup>4</sup>
$I_{bt}$	Beams torsional inertia	$0.480 \cdot 10^{-7}$	m <sup>4</sup>

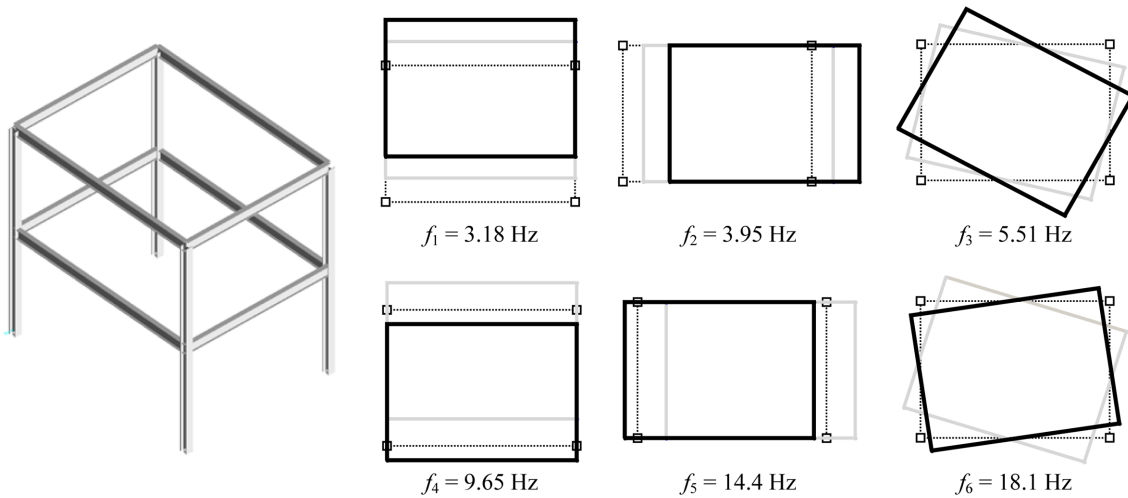


Fig. 3 The FE baseline model (BC configuration): (left) axonometric view, (right) planar schematization of the mode-shapes

#### 4. The experimental modal identification: errors in the model structure

The experimental modal model is identified on the basis of ambient vibration tests. Many output-only identification techniques have been developed in the past few years for use in ambient vibration conditions. They are widely applied to full-scale civil structures, where forced vibration testing and free vibration testing are typically precluded by the difficulties of imparting large external loads under normal operational conditions. Several review papers concerning the state-of-the-art identification methods and recent developments are present in the scientific literature (Maia

and Silva 1997). A certain effort is recognized to produce qualitative and quantitative comparisons among different methods, mostly based on experimental or pseudo-experimental data from benchmark structures (Giraldo *et al.* 2009).

Modal identification methods generally fall into two categories, depending on whether they operate in the time domain or in the frequency domain. Hybrid methods operating in the joint time-frequency domain have also been recently developed. The applicability and success of a given method depend on a variety of aspects, including the expected structural peculiarities (modal density, damping ratios, nonlinearities), the target results (modal model order, completeness) and finally the nature (periodicity, stationarity) and quality (noise-to-signal ratio) of the available data (Peeters and Ventura 2003).

In this study, three classical output-only methods are used, respectively working in the time-domain, in the frequency-domain and in the time-frequency domain: ERA (Eigensystem Realization Algorithm) (Juang and Pappa 1984), FDD (Frequency Domain Decomposition) (Brincker *et al.* 2001) and TFIE (Time-Frequency Instantaneous Estimators) (Bonato *et al.* 2000). The accelerations measured by the 8 sensors placed at the first and second levels are used for identification. By

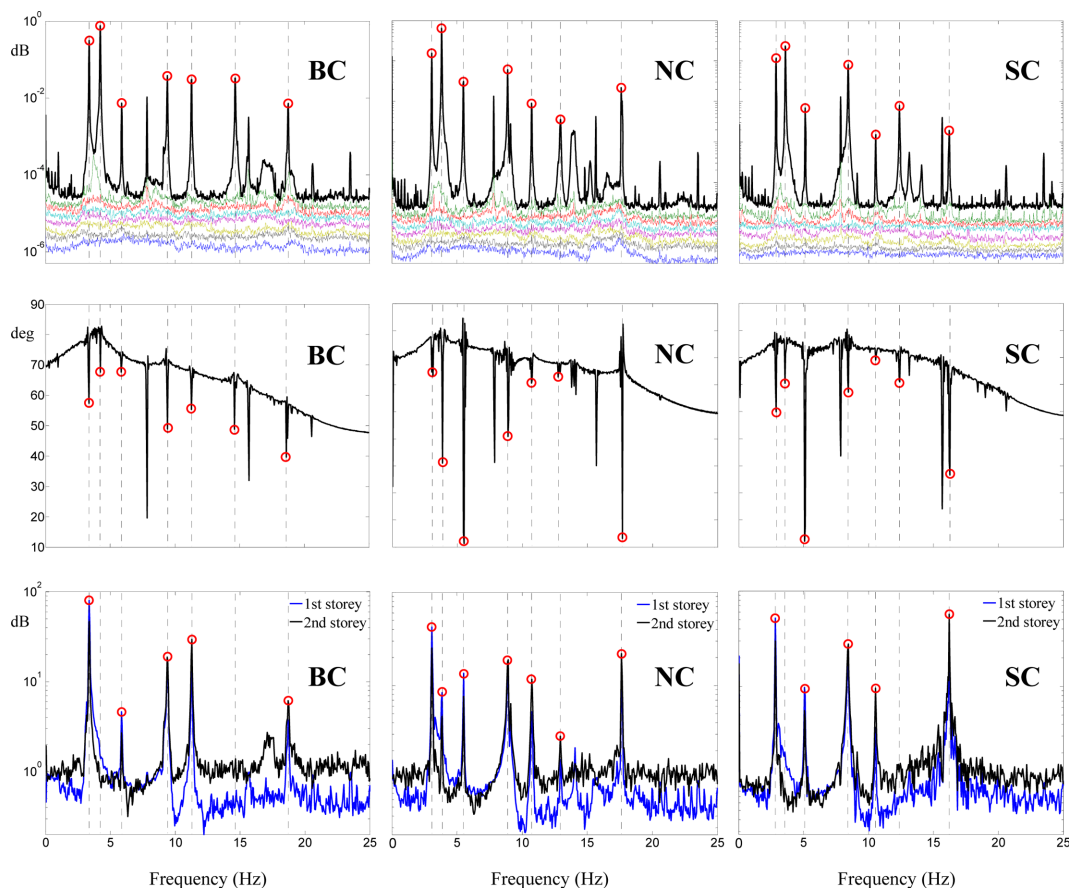


Fig. 4 Modal frequency identification for, respectively, the BC (left), NC (centre) and SC (right) configurations: (top) FDD singular values; (middle) TFIE phase difference standard deviations; (bottom) TFs from the ground to the two storey levels in the along- $y$  direction

enforcing the assumption of rigid in-plan motion of each floor so as to reduce (in a least-square sense) measurement data to the 6 DOFs of the analytical model, 6-components eigenvectors are finally synthesized. Transfer Functions (TFs) are also computed from the accelerations measured at the ground level to the accelerations measured at other locations, in order to verify the presence of spurious frequency components inherent in ground vibration. In order to minimize measurement and processing errors, each method is first applied to several data fragments and then the experimental modal model is obtained as the average over the whole of data fragments and the whole of the three methods. By repeating the procedure for each of the three mass configurations, the resulting experimental modal model is finally obtained, consisting (like its analytical counterpart) of a triplet of eigen-frequency vectors  $\mathbf{f}_e$  and a triplet of eigen-mode matrices  $\Phi_e$  (the “e” subscript standing for “experimental”).

Fig. 4 exemplifies the modal identification procedure on a single fragment of data. The three top sub-figures show the FDD singular value curves, with the structural natural frequencies identified through peak-picking (red circles), for respectively the BC, the NC and the SC mass configurations. Similarly, the three central sub-figures show the TFIE standard deviations of the phase difference. Unexpectedly, seven natural frequencies are identified. Same results are obtained using the ERA method (no graphical output is available in this case). Finally, the three bottom sub-figures contain the TFs from the ground acceleration to the acceleration at respectively the first and the second floors.

Table 3 Experimental modal properties – Mean values (%o standard deviation in brackets)

Conf.	Mode	$f_{ei}$ (Hz)	$\phi_{ei1}$	$\phi_{ei2}$	$\phi_{ei3}$	$\phi_{ei4}$	$\phi_{ei5}$	$\phi_{ei6}$
BC	1	3.37 (.3)	-.009	.507 (6)	.001	-.005	.862 (2)	.004
	2	4.23 (.6)	.445 (2)	-.004	-.002	.895 (0)	.006	.000
	3	5.89 (.2)	.057	.053	.478 (84)	.054	-.011	.873 (7)
	4a	9.39 (.6)	.026	.777 (27)	.006	-.038	-.627 (31)	-.029
	4b	11.3 (.2)	-.031	.913 (10)	.006	-.020	-.405 (69)	-.010
	5	14.6 (.1)	.876 (5)	.000	.004	-.483 (15)	.005	-.005
NC	6	18.7 (.1)	-.006	-.071	.828 (30)	-.006	.011	-.555 (41)
	1	3.08 (.5)	-.004	.510 (9)	.005	-.007	.860 (3)	.004
	2	3.85 (.7)	.448 (3)	-.004	.027	.892 (1)	.002	.049
	3	5.51 (.6)	-.120	.010	.470 (12)	-.276	-.032	.829 (8)
	4a	8.90 (.4)	.012	.825 (5)	.000	.004	-.565 (10)	-.017
	4b	10.7 (.1)	.020	.927 (7)	.011	.022	-.372 (23)	-.020
SC	5	12.9 (.3)	.868 (0)	-.081	.084	-.475 (58)	.027	-.082
	6	17.6 (.0)	-.247	-.011	.806 (8)	.196	.021	-.501 (10)
	1	2.85 (.5)	-.004	.505 (6)	-.001	-.004	.863 (3)	.005
	2	3.57 (.6)	.447 (4)	-.002	-.001	.894 (1)	.007	-.001
	3	5.11 (.1)	-.005	.012	.495 (39)	.019	-.015	.868 (18)
	4a	8.43 (.4)	.003	.840 (5)	.002	-.004	-.542 (9)	-.012
SC	4b	10.5 (.1)	-.001	.944 (8)	.001	-.006	-.329 (65)	-.011
	5	12.4 (.2)	.880 (7)	-.005	.002	-.474 (24)	.002	-.004
	6	16.2 (.1)	-.016	-.062	.851 (12)	.022	.008	-.520 (24)

Table 3 reports the mean values of the experimental natural frequencies and mode-shape components, together with the corresponding normalized standard deviations (expressed in per-thousand). The normalized standard deviation is very small for the natural frequencies (never larger than 0.7‰) and quite small too for the main mode-shape components (ranging from less than 1‰ to 84‰). Not reported in Table 3 and out of the scope of the present paper, modal damping around 2-3‰ is obtained for all modes.

An interesting anomaly in Fig. 4 and Table 3, clearly incompatible with the assumed 6-DOF model structure, is the occurrence, instead of the expected fourth mode, of two distinct experimental modes, denoted as 4a and 4b, having similar modal shapes but well-separated modal frequencies. In the BC configuration, modes 1, 4a and 4b are flexural modes in the transverse direction, modes 2 and 5 are flexural modes in the longitudinal direction, modes 3 and 6 are torsional modes. More specifically, modes 1, 2 and 3 are in-phase modes, whilst modes 4a, 4b, 5 and 6 are counter-phase modes. In the NC configuration, due to the eccentricity of the additional masses along the transverse direction, a weak lateral-torsional coupling arises between the flexural modes in the longitudinal direction and the torsional modes, so that rotational components appear in modes 2 and 5, and flexural components in modes 3 and 6. Also, due to the increased mass, the natural frequencies systematically decrease. In the SC configuration, lateral-torsional coupling vanishes because of the recovered double symmetry, and natural frequencies become even smaller because of the further mass increment.

In order to explain the origin of modes 4a and 4b, the question first arises if they are real modes, reflecting the true dynamic signature of the structural system, or spurious modes, caused by testing or identification inaccuracies. An example of spurious frequency is the peak at 7.8 Hz visible in the FDD plots and TFIE plots in Fig. 4, which can be easily attributed to frequency components inherent in the external input, i.e., the ground acceleration. In fact, several circumstances proclaim modes 4a and 4b as real modes. They are confirmed by all identification sessions, independently of the data fragment, the identification method, the mass configuration, and the vibration intensity. They undergo the same trend of frequency reduction recognizable in any other mode as the structural mass increases (the spurious peak at 7.8 Hz is instead unaffected by mass variations). They are not the effect of abnormal frequency components in the external input, as confirmed by the acceleration auto-spectra at the base level (see Fig. 5 next). In conclusion, modes 4a and 4b can be confidently classified as real structural modes. But what's their origin then?

To answer, let us consider Fig. 5, which plots the auto-spectral densities of the acceleration signals

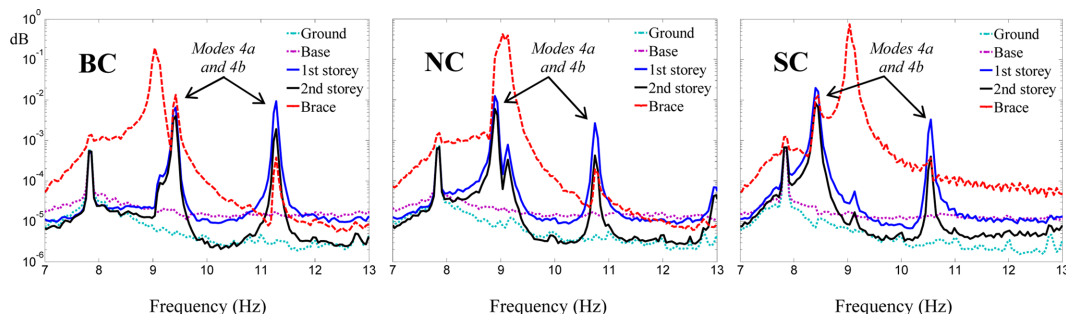


Fig. 5 Auto-spectral densities in the along- $y$  direction for, respectively, the BC (left), NC (centre) and SC (right) configurations

recorded along the transverse direction at, respectively, the ground level, the base level, the first and second floor levels and the gusset plate atop one of the lower V-inverted braces (i.e., those attached to the base level).

Firstly, a confirmation is obtained of the real nature of modes 4a and 4b: the two respective peaks, migrating leftwards as the structural mass increases, are prominent in the spectra corresponding to the two storey levels whilst are nearly absent from the spectra corresponding to the ground level and to the base level, in contrast with the small peak around 7.8 Hz (already classified as a spurious frequency), which appears almost identical for all spectra and independent of the mass configuration.

Besides, Fig. 5 draws attention to the so far neglected influence of the V-inverted braces. These can be classified as secondary structural elements. Their mass is small, their connection to the main frame is uncertain, their transverse (out-of-plane) dynamics is of scarce interest in the final (controlled) structural configuration. Accordingly, their dynamics was omitted in the formulation of the simplified 6-DOF model structure. Fig. 5 shows that this omission is questionable. Firstly, coupling is observed between the spectrum corresponding to the brace and the spectra corresponding to the first and second storeys: modes 4a and 4b produce high peaks in the brace spectrum, and on its turn the brace causes small but distinct perturbations in the structural spectra. Such interaction is even more remarkable in that it regards one of the lower braces (the only instrumented one, unfortunately), which are attached to the base level. Secondly, the natural frequency of the out-of-phase local mode of the instrumented lower brace is shown to be close to modes 4a and 4b, and approximately equal to 9 Hz.

These findings allow a nice physical interpretation of modes 4a and 4b, based on the well-known concept of tuned mass dampers (TMDs). A TMD is a passive absorber working as an SDOF appendage of the main system (Den Hartog 1956). Setting the frequency ratio  $r_b$  (defined as the frequency of the TMD divided by the frequency of the structural “target mode”) close to one ensures an energy transfer from the target mode to the absorber as a consequence of a phenomenon of dynamic interaction or *modal tuning*. Consequently, instead of the single target frequency of the original (uncontrolled) system, the controlled system possesses two natural frequencies, resulting in two spectral peaks, one right below and one right above the original peak. The smaller  $r_b$ , the higher the second peak with respect to the first peak, and vice versa. Also, the smaller the absorber damping ratio, the sharper the two peaks.

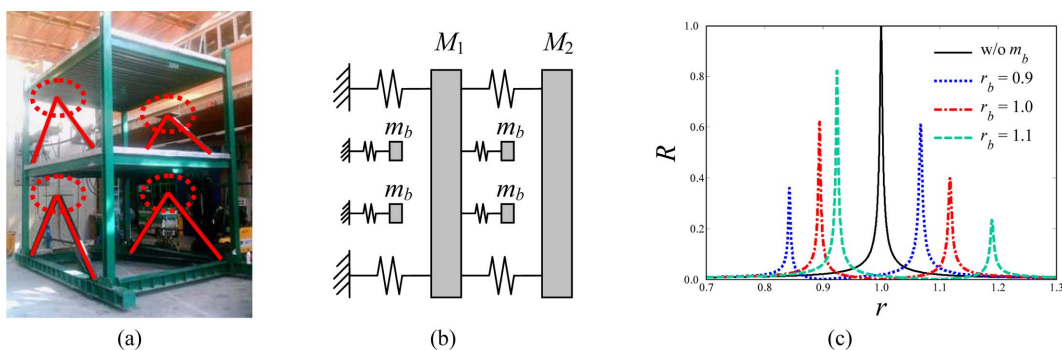


Fig. 6 V-inverted braces working as tuned appendages: (a) location of the V-inverted braces crowned with gusset plates; (b) schematics of the mechanical model in the  $y$  direction including braces dynamics; (c) typical FRF for an SDOF system with and w/o an under-damped tuned appendage

All ingredients being set, the explanation of modes 4a and 4b is straightforward and schematized in Fig. 6. The two modes result from the dynamic interaction between the fourth mode of the main frame and the out-of-plane mode of the upper braces (those attached to the first floor, unfortunately not instrumented), by chance working as a couple of under-damped TMDs roughly tuned to the benchmark structure. The total mass of the two TMDs, including the two gusset plates atop and approximately half the mass of the braces, is around 140 kg. This value, apparently small if compared with the total mass of the building (approximately 6600 kg), is indeed large enough if compared with the modal mass of the fourth mode (approximately 500 kg according to the subsequent calibration), thus justifying the strong modal coupling. An interesting confirmation comes from the spectra of the first and second storeys in Fig. 5. As the mass increases from the BC to the NC and further to the SC configurations, the frame structural frequencies obviously decrease whilst the frequency of the couple of (unobserved) TMDs remains unchanged. This is equivalent to increasing the frequency ratio  $r_b$  and consequently, as sketched in Fig. 6(c), to making the left spectral peak prevail over the right one. This very effect is experimentally recognizable in Fig. 5, where the left spectral peak (mode 4a) tends to increasingly prevail over the right spectral peak (mode 4b) while moving from the BC to the SC configuration. A further, decisive confirmation, not available at the time when the model updating was first performed, was obtained later on, when an accelerometer placed on one of the upper braces revealed an out-of-plane frequency close to 10 Hz, right in the middle between the natural frequencies of modes 4a and 4b.

In conclusion, the experimental modal identification of the benchmark prototype reveals the insurgence of two unexpected resonant modes (4a and 4b) as the consequence of the interaction between the main structure and the upper V-inverted braces. Such explanation has required a considerable deal of physical insight because the resonant braces were not instrumented during testing. To the authors' knowledge, this is the first time that such accidental modal tuning is observed between a frame building structure and secondary structural elements. Obviously the two resonant modes can not be captured by the simplified 6-DOF analytical model, which in fact renounces simulating brace dynamics. In order to face such an error in the model structure, two main options are available. The first one, left for future work, is the removal of the modelling error, i.e., the inclusion of the braces into the model. The second one, pursued in this work, is an *experimental model reduction* (contrary to the classical *analytical model reduction*) consisting in the removal of the resonant modes from the experimental data. In this way, the FE model is calibrated relying exclusively on matching the five modes which do not feel the effect of modal tuning. This approach, which obviously can not be regarded as a general methodology to deal with modelling errors, appears nonetheless one viable strategy whenever the effects of unmodelled structural elements are known to be confined to a circumscribed region of the experimental data, and this region does not need to be accurately replicated by the model.

## 5. FE model-updating: errors in the model parameters

### 5.1 Multi-model parameterization

The key to success in model calibration is the choice of the updating parameters. Any choice of the updating set will implicitly introduce some modelling errors in regions of the model which are excluded from updating (Sanayei *et al.* 2001). Clearly, from the point of view of conditioning, it

would be best to select a small number of parameters for updating, and to use large volumes of measured data. On the contrary, if data were rich enough, and errors in measurement and processing as well as errors in the model structure were ideally absent, then it would be more convenient to enlarge as much as possible the updating set in order to correct erroneous assumptions. In general, updating parameters should be chosen so that the measured data are sensitive to them, but also there should be clear indication that there might be modelling errors in the corresponding regions of the model. This typically requires the application of a great deal of physical insight, and the use of any *a priori* knowledge available about the actual system.

However, *a priori* knowledge alone is often insufficient to directly identify the optimal updating set, and more typically ends up with suggesting a whole family of candidate options. In such cases, multi-model reasoning may prove a useful strategy to explore and compare potential candidates (Robert-Nicoud *et al.* 2005, Raphael and Smith 2003, Zarate and Caicedo 2008).

In this paper, a multi-model parameterization approach is proposed consisting in the generation and solution of a multitude of models, characterized by the same model structure but by different updating sets.

More specifically, supposing an adequate model structure has already been chosen, the procedure develops through the following steps:

- Step 1: a meaningful objective (or error) function  $f_{ob}$  is selected, quantifying the discrepancy between the experimental and the analytical models (residual);
- Step 2: a robust optimization algorithm is chosen, capable to reliably minimize the objective function;
- Step 3: the total set  $\mathbf{p} \in \mathcal{R}^{N_p}$  of the *potential updating parameters* is identified, based on the evaluation of the sensitivity of the objective function to changes in model parameters (sensitivity analysis) and/or on the *a priori* estimation of their respective uncertainties; in the case of large FE models, the total set  $\mathbf{p}$  may be profitably identified through applying parameterization techniques based on sub-structuring (Kim and Park 2008, Perera and Ruiz 2008, Adhikari and Friswell 2010);
- Step 4: the total set  $\mathbf{p}$  is partitioned into two subsets: the set of *updating parameters*, denoted as  $\mathbf{p}_u \in \mathcal{R}^{N_u}$ , and its complementary set of *constrained parameters*, denoted as  $\mathbf{p}_c \in \mathcal{R}^{N_p - N_u}$ ; while  $\mathbf{p}_u$  contains the independent optimization variables,  $\mathbf{p}_c = \mathbf{F}(\mathbf{p}_u)$  contains the parameters which are excluded from updating, equalled either to their respective nominal value or, more generally, to any possible function  $\mathbf{F}$  of  $\mathbf{p}_u$ ; such partition will be called a model, and denoted as  $\mathcal{M}_i (N_u)$ ;
- Step 5: the model defined at Step 4 is optimally updated, i.e.,  $\mathbf{p}_u$  is found which minimizes  $f_{ob}$ ;
- Step 6: Steps 4 and 5 are iterated, each time selecting a different updating set (i.e., a different model), e.g., enlarging previous sets by progressively including new parameters until reaching under-determinacy;
- Step 7: the multiple models are compared and the one(s) which sound(s) more reliable according to the engineering experience is(are) selected to represent the real structure.

This approach has contact points with existing strategies of direct-search multi-model updating, especially the one developed at EPFL (Saitta *et al.* 2005, Raphael and Smith 2003). The main common feature is the idea of generating alternative solutions to increase identification robustness. But there are also significant differences. The EPFL method identifies a set of “good” models (i.e., sub-optimal models, encountered while searching for optimality, whose residuals lie below a specified threshold) and then automatically classify them into multiple clusters, each representing a candidate solution. Implicit is the assumption that errors in measurements and in model structure are

relatively large with respect to errors in model parameters, so that the analytical global optimum retain little physical significance; provided that the analyst can estimate the extent of measurement and modelling errors and evaluate a proper threshold for the admissible residual, all models respecting that threshold are regarded as equally admissible candidates. The present approach, instead, identifies distinct global optima, one for each updating set, and tracks their evolution as the updating set enlarges towards non-uniqueness. Implicit is the assumption that errors in measurements and in model structure are either acceptably small with respect to errors in model parameters (as plausibly happens in the present case study because of the simple structural configuration and the redundancy/controllability of measured data) or anyway so unpredictable that no reliable estimation of the threshold error is possible.

## 5.2 Application to the case study

In this paragraph, the 7-step procedure outlined above is applied to the benchmark case study.

### 5.2.1 Step 1

The objective function is introduced as the following normalized modal residual

$$f_{ob} = \sqrt{\frac{\sum_i [(f_i/f_{ei} - 1)^2 + \lambda^2 (\sqrt{2(1 - \sqrt{\text{MAC}_{ii}})})^2]}{\sum_i (1 + \lambda^2)}} \quad (1)$$

where the summations extend to all modes but the fourth one and to all mass configurations;  $f_i$  and  $f_{ei}$  are respectively the analytical and the experimental natural frequencies;  $\text{MAC}_{ii}$  is the Modal Assurance Criterion between the analytical mode-shape  $\phi_i$  and the corresponding experimental mode-shape  $\phi_{ei}$ ; the term  $f_i/f_{ei} - 1$  accounts for the frequency residual, while the term  $\sqrt{2(1 - \sqrt{\text{MAC}_{ii}})}$  accounts for the mode-shape residual, geometrically representing the Euclidean distance between vectors  $\phi_i$  and  $\phi_{ei}$  (normalized so as to have unit Euclidean length);  $\lambda = 0.1$  is a relative weight assigned to the mode-shapes residuals, roughly accounting for the different reliability of mode-shape information with respect to frequency information. Eq. (1) is so conceived that when all residuals equal a certain value, then  $f_{ob}$  equals the same value. In this sense,  $f_{ob}$  is the weighted error of the analytical modal model with respect to the experimental modal model.

### 5.2.2 Step 2

Optimization is performed through a hybrid direct-search algorithm, consisting of a genetic algorithm (GA) followed by a nonlinear least-square solver (a subspace trust region method based on the interior-reflective Newton method) (Jung and Kim 2009). The GA ensures robustness of the solution (i.e., its closeness to the global optimum), the least-square solver locally improves its accuracy.

### 5.2.3 Step 3

The total set  $\mathbf{p}$  of potential updating parameters is easily identified in the present case. Given the simplified structure of the FE model and admitting a substantial in-plan symmetry of the bare frame, 8 stiffness parameters and 4 mass parameters completely characterize the model (the rotational stiffness of columns and beams has negligible effects on modal response). Normalized to

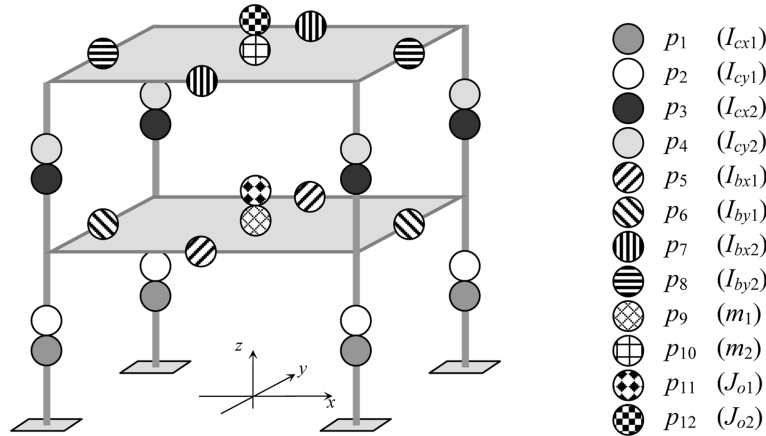


Fig. 7 The FE model with the 12 potential updating parameters

their respective nominal values, the  $N_p = 12$  parameters are described in Fig. 7 and include: 4 parameters,  $p_1$  to  $p_4$ , representing column bending inertias ( $I_{cx1}, I_{cy1}, I_{cx2}, I_{cy2}$ ); 4 parameters,  $p_5$  to  $p_8$ , representing beam bending inertias ( $I_{bx1}, I_{by1}, I_{bx2}, I_{by2}$ ); and 4 parameters,  $p_9$  to  $p_{12}$ , representing slab masses and polar inertias ( $m_1, m_2, J_{o1}, J_{o2}$ ).

### 5.2.4 Steps 4 to 7

Alternative subsets of the 12 parameters, i.e., alternative models, are considered and separately solved. The number  $N_u$  of the updating parameters is varied from a minimum of 2 to a maximum of 12. The case  $N_u = 0$  is also included for comparison, corresponding to the nominal model.

Depending on  $N_u$ , two qualitatively different situations are met, corresponding to, respectively, a determinate and an under-determinate inverse problem.

In what follows, nine different models are first considered having  $N_u \leq 10$ , each admitting a unique solution (determinate case). Then, the problem is demonstrated to be under-determinate for  $N_u > 10$  and some of the  $\infty^2$  solutions corresponding to  $N_u = 12$  are presented.

Table 4 The updating parameters for the nine candidate models

Model	$N_u$	$p_1$ ( $I_{cx1}$ )	$p_2$ ( $I_{cy1}$ )	$p_3$ ( $I_{cx2}$ )	$p_4$ ( $I_{cy2}$ )	$p_5$ ( $I_{bx1}$ )	$p_6$ ( $I_{by1}$ )	$p_7$ ( $I_{bx2}$ )	$p_8$ ( $I_{by2}$ )	$p_9$ ( $m_1$ )	$p_{10}$ ( $m_2$ )	$p_{11}$ ( $J_{o1}$ )	$p_{12}$ ( $J_{o2}$ )
$\mathcal{M}_{0(0)}$	0	1	1	1	1	1	1	1	1	1	1	1	1
$\mathcal{M}_{1(2)}$	2	$p_{u1}$	$p_{u1}$	1	1	1	1	1	1	$p_{u2}$	$p_{u2}$	$p_{u2}$	$p_{u2}$
$\mathcal{M}_{2(3)}$	3	$p_{u1}$	$p_{u2}$	1	1	1	1	1	1	$p_{u3}$	$p_{u3}$	$p_{u3}$	$p_{u3}$
$\mathcal{M}_{3(3)}$	3	$p_{u1}$	$p_{u1}$	1	1	1	1	1	1	$p_{u2}$	$p_{u3}$	$p_{u2}$	$p_{u3}$
$\mathcal{M}_{4(4)}$	4	$p_{u1}$	$p_{u2}$	1	1	1	1	1	1	$p_{u3}$	$p_{u4}$	$p_{u3}$	$p_{u4}$
$\mathcal{M}_{5(6)}$	6	$p_{u1}$	$p_{u2}$	1	1	1	1	1	1	$p_{u3}$	$p_{u4}$	$p_{u5}$	$p_{u6}$
$\mathcal{M}_{6(8)}$	8	$p_{u1}$	$p_{u2}$	$p_{u3}$	$p_{u4}$	1	1	1	1	$p_{u5}$	$p_{u6}$	$p_{u7}$	$p_{u8}$
$\mathcal{M}_{7(8)}$	8	$p_{u1}$	$p_{u2}$	1	1	$p_{u3}$	$p_{u4}$	$p_{u3}$	$p_{u4}$	$p_{u5}$	$p_{u6}$	$p_{u7}$	$p_{u8}$
$\mathcal{M}_{8(10)}$	10	$p_{u1}$	$p_{u2}$	$p_{u3}$	$p_{u4}$	$p_{u5}$	$p_{u6}$	$p_{u5}$	$p_{u6}$	$p_{u7}$	$p_{u8}$	$p_{u9}$	$p_{u10}$

The determined case:  $N_{it} \leq 10$

Nine different models are explored, summarized in Table 4:

- $\mathcal{M}_{0(0)}$  is the nominal model;
- $\mathcal{M}_{1(2)}$  depends on 2 parameters, i.e., the stiffness of lower columns and the mass properties of the floors; note: (i) two is the minimum number of parameters to simultaneously update stiffness and mass of the model; (ii) stiffness uncertainty is attributed entirely to the lower columns because the main modelling uncertainty is recognized in the assumption of perfect clamping at the base of the columns;
- $\mathcal{M}_{2(3)}$  depends on 3 parameters, i.e., the stiffness of lower columns, respectively in the longitudinal and transverse directions, and the mass properties of the floors; note: (i) with respect to  $\mathcal{M}_{1(2)}$ , the degree of clamping at the base of the columns is differentiated along the two directions;
- $\mathcal{M}_{3(3)}$  still depends on 3 parameters, i.e., the stiffness of lower columns and the mass properties of the first and the second floors; note: (i) with respect to  $\mathcal{M}_{1(2)}$ , the two floors are allowed different masses;
- $\mathcal{M}_{4(4)}$  depends on 4 parameters, obtained as the *union* of the sets corresponding to  $\mathcal{M}_{2(3)}$  and  $\mathcal{M}_{3(3)}$ ;
- $\mathcal{M}_{5(6)}$  depends on 6 parameters, obtained from  $\mathcal{M}_{4(4)}$  by further making slab polar inertias independent of slab masses; note: (i)  $\mathcal{M}_{5(6)}$  independently allows for the contributions of, respectively, the uniform slab thickness and the additional sagging deflection; (ii) from here on, the four mass parameters will be systematically included in any new updating set, i.e., the mass matrix  $\mathbf{M}$  will depend on all four mass parameters; (iii) the stiffness matrix  $\mathbf{K}$  still depends on the stiffness of lower columns only;
- $\mathcal{M}_{6(8)}$  depends on 8 parameters, obtained from  $\mathcal{M}_{5(6)}$  by further including the stiffness of upper columns in both directions; note: (i)  $\mathbf{K}$  now depends on all column stiffness parameters; (ii) beam stiffness is still taken as nominal;
- $\mathcal{M}_{7(8)}$  still depends on 8 parameters, obtained from  $\mathcal{M}_{5(6)}$  by further including beam stiffness in both directions; note: (i)  $\mathbf{K}$  now depends on the stiffness of lower columns and on beam stiffness, the latter being assumed independent of the storey level ( $p_7 = p_5$  and  $p_8 = p_6$ );
- $\mathcal{M}_{8(10)}$  depends on 10 parameters, obtained as the *union* of the sets corresponding to  $\mathcal{M}_{6(8)}$  and  $\mathcal{M}_{7(8)}$ ; note: (i) all potential parameters in  $\mathbf{p}$  are taken as independent variables, except the beam bending inertias, constrained by the equalities  $p_7 = p_5$  and  $p_8 = p_6$ .

Table 5 The solutions obtained with the multiple models

Model	$p_1$ ( $I_{cx1}$ )	$p_2$ ( $I_{cy1}$ )	$p_3$ ( $I_{cx2}$ )	$p_4$ ( $I_{cy2}$ )	$p_5$ ( $I_{bx1}$ )	$p_6$ ( $I_{by1}$ )	$p_7$ ( $I_{bx2}$ )	$p_8$ ( $I_{by2}$ )	$p_9$ ( $m_1$ )	$p_{10}$ ( $m_2$ )	$p_{11}$ ( $J_{o1}$ )	$p_{12}$ ( $J_{o2}$ )	$f_{ob}$ (%)
$\mathcal{M}_{0(0)}$	1	1	1	1	1	1	1	1	1	1	1	1	4.26
$\mathcal{M}_{1(2)}$	.751	.751	1	1	1	1	1	1	.770	.770	.770	.770	2.48
$\mathcal{M}_{2(3)}$	.623	.731	1	1	1	1	1	1	.710	.710	.710	.710	1.90
$\mathcal{M}_{3(3)}$	.830	.830	1	1	1	1	1	1	.932	.742	.932	.742	1.08
$\mathcal{M}_{4(4)}$	.755	.795	1	1	1	1	1	1	.878	.716	.878	.716	1.01
$\mathcal{M}_{5(6)}$	.756	.792	1	1	1	1	1	1	.887	.716	.830	.694	.856
$\mathcal{M}_{6(8)}$	.782	.778	1.07	.915	1	1	1	1	.862	.726	.834	.707	.843
$\mathcal{M}_{7(8)}$	.629	.755	1	1	1.25	1.19	1.25	1.19	.816	.777	.790	.740	.780
$\mathcal{M}_{8(10)}$	.620	.739	.956	.964	1.28	1.28	1.28	1.28	.794	.783	.757	.749	.775

Table 6 Mutual distances  $d_{ij}$  in the search space (%)

	$\mathcal{M}_{0(0)}$	$\mathcal{M}_{1(2)}$	$\mathcal{M}_{2(3)}$	$\mathcal{M}_{3(3)}$	$\mathcal{M}_{4(4)}$	$\mathcal{M}_{5(6)}$	$\mathcal{M}_{6(8)}$	$\mathcal{M}_{7(8)}$	$\mathcal{M}_{8(10)}$
$\mathcal{M}_{0(0)}$	0	16.7	21.4	12.9	15.6	16.3	16.2	22.3	24.8
$\mathcal{M}_{1(2)}$		0	5.10	7.44	5.07	4.80	5.21	13.6	16.7
$\mathcal{M}_{2(3)}$			0	11.3	8.04	7.48	8.09	13.7	16.6
$\mathcal{M}_{3(3)}$				0	3.42	4.32	5.28	15.4	18.7
$\mathcal{M}_{4(4)}$					0	1.54	3.63	14.0	17.4
$\mathcal{M}_{5(6)}$						0	3.45	13.9	17.3
$\mathcal{M}_{6(8)}$							0	14.3	17.6
$\mathcal{M}_{7(8)}$								0	4.18
$\mathcal{M}_{8(10)}$									0

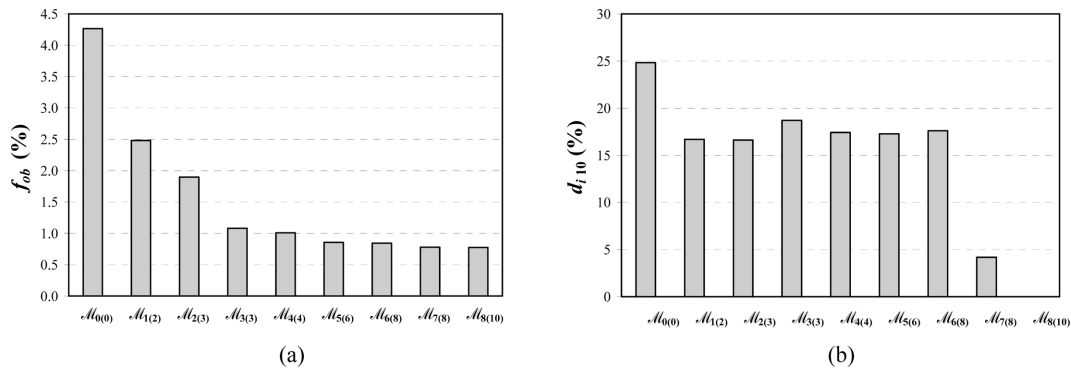


Fig. 8 Comparison among the multiple models: (a) objective function; (b) distance from  $\mathcal{M}_{8(10)}$  in the search space

For all nine models above except  $\mathcal{M}_{0(0)}$  optimization is run several times in order to avert the risk of non-uniqueness of the solution. Excellent reproducibility is observed in all cases. Results are reported in Table 5.

Table 6 evaluates the mutual distance among the nine models in the search domain, where the distance  $d_{ij}$  between any two models  $i$  and  $j$  is defined as the Euclidean distance between the corresponding vectors  $\mathbf{p}_i$  and  $\mathbf{p}_j$ , further divided by the square root of  $N_p$ . Fig. 8 compares the 9 models in terms of, respectively, the objective function (on the left) and the distance from model  $\mathcal{M}_{8(10)}$  in the search space (on the right).

Results in Tables 5 and 6 and in Fig. 8 suggest the following comments:

- Expectedly, increasing  $N_u$  improves fitting the experimental data. The nominal model,  $\mathcal{M}_{0(0)}$ , has the worst fitting capability ( $f_{ob} = 4.26\%$ ) while the ten parameters model,  $\mathcal{M}_{8(10)}$ , has the best one ( $f_{ob} = 0.775\%$ ). Recalling that  $f_{ob}$  is the average error in replicating the experimental modal response, these values appear quite low for a civil application (Zarate and Caicedo 2008), plausibly because of the simplicity of the structural configuration and the controllability of test conditions. The decreasing trend of  $f_{ob}$  is pronounced for small values of  $N_u$  but tends to vanish as  $N_u$  increases. If considered in absolute terms, the objective function improvement from  $\mathcal{M}_{5(6)}$  to  $\mathcal{M}_{8(10)}$  is seemingly unsubstantial; to be properly appreciated, it must be considered in relative

terms ( $f_{ob}$  reduces 1.10 times from  $\mathcal{M}_{5(6)}$  to  $\mathcal{M}_{8(10)}$ ).

- In order to genuinely capture the improvement of the model, however, the search space must be examined too and the multiple solutions must be compared in terms not only of their fitting capability but also of the plausibility of the underlying parametric description. A reduced objective function does not necessarily mean approaching the “true” model in the search space. This clearly appears from Fig. 8: moving from  $\mathcal{M}_{0(0)}$  to  $\mathcal{M}_{8(10)}$ ,  $f_{ob}$  monotonically decreases whilst the average distance of each model from  $\mathcal{M}_{8(10)}$  shows an irregular trend, keeping nearly constant (or even slightly increasing) from  $\mathcal{M}_{1(2)}$  to  $\mathcal{M}_{6(8)}$ , and significantly diminishing only at  $\mathcal{M}_{7(8)}$ . Supposing  $\mathcal{M}_{8(10)}$  were the “true” model (this point will be reconsidered later), model  $\mathcal{M}_{6(8)}$  would result as distant from “truth” as model  $\mathcal{M}_{1(2)}$ . Such distance, which represents the average parameter error, is conspicuous for all models (larger than 16%) except model  $\mathcal{M}_{7(8)}$  (about 4%), implying that remarkably different models exist providing similar objective functions (ill-conditioning).

- Two strategies may be devised to deal with such multiple candidates. The first strategy assumes that all models whose objective function is below a determined threshold (e.g.,  $\mathcal{M}_{5(6)}$ ,  $\mathcal{M}_{6(8)}$ ,  $\mathcal{M}_{7(8)}$  and  $\mathcal{M}_{8(10)}$ ) are equally admissible representations of the physical system (Saitta *et al.* 2005, Raphael and Smith 2003). The second strategy relies on engineering insight to state the plausibility of each candidate and isolate the most likely one(s). For example, model  $\mathcal{M}_{3(3)}$ , despite its lower objective function, can be recognized as an involution of model  $\mathcal{M}_{2(3)}$ : starting from the unlikely assumption that the effects of imperfect clamp at the column base are the same along the two in-plan directions ( $p_1 = p_2$ ),  $\mathcal{M}_{3(3)}$  provides a solution which, through unrealistically increasing the first floor mass ( $p_9 = 0.932$ ) while decreasing the second floor mass ( $p_{10} = 0.742$ ), is clearly incompatible with visual inspections; as a confirmation of such involution, model  $\mathcal{M}_{3(3)}$  is the most distant from  $\mathcal{M}_{8(10)}$  among all updated models.

- Applied to the four models which best fit experiments, i.e.,  $\mathcal{M}_{5(6)}$ ,  $\mathcal{M}_{6(8)}$ ,  $\mathcal{M}_{7(8)}$  and  $\mathcal{M}_{8(10)}$ , the second strategy allows explaining their differences and rejecting improbable models. So  $\mathcal{M}_{5(6)}$  ( $f_{ob} = 0.856\%$ ) makes the stiffness matrix depend only on the stiffness of lower columns, achieving poor approximation.  $\mathcal{M}_{6(8)}$  ( $f_{ob} = 0.843\%$ ) slightly improves fitting by including two additional variables, i.e., the stiffness of upper columns, but the improvement is more seeming than real because upper and lower columns are in fact a unique structural element and the stiffness of upper columns is expected to negligibly deviate from its nominal value.  $\mathcal{M}_{7(8)}$  ( $f_{ob} = 0.780\%$ ) is considerably superior to both  $\mathcal{M}_{5(6)}$  and  $\mathcal{M}_{6(8)}$ , because in this case the two additional variables, representing the beam stiffness, possess a larger degree of uncertainty than that related to the upper columns. In the updated  $\mathcal{M}_{7(8)}$  model, the stiffness of lower columns is less than nominal because of the imperfect clamp at the base while the beam stiffness is larger than nominal because of the partial collaboration of the floor slabs. Finally  $\mathcal{M}_{8(10)}$  ( $f_{ob} = 0.775\%$ ), which enlarges the updating set to both the upper columns stiffness and the beams stiffness, obviously improves all previous models in terms of the objective function. From a physical viewpoint,  $\mathcal{M}_{8(10)}$  is characterized by a very convincing set of updated parameters, with a substantial uniformity in both beam stiffness and mass properties, and with the stiffness of upper columns only slightly reduced with respect to their nominal value. In conclusion, the updated  $\mathcal{M}_{8(10)}$  model possesses enough fitting capabilities and sufficiently sound physical meaning to be accepted as a reliable representation of the benchmark structure. Table 7 and 8 report, respectively, its modal properties and its residuals.

The under-determined case:  $N_u > 10$

Table 7 Analytical modal properties of the updated  $\mathcal{M}_{8(10)}$  model

Conf.	Mode	$f_i$ (Hz)	$\phi_{i1}$	$\phi_{i2}$	$\phi_{i3}$	$\phi_{i4}$	$\phi_{i5}$	$\phi_{i6}$
BC	1	3.38	.000	.510	.000	.000	.860	.000
	2	4.24	.463	.000	.000	.886	.000	.000
	3	5.87	.000	.000	.486	.000	.000	.874
	4	10.1	.000	.853	.000	.000	-.522	.000
	5	14.5	.880	.000	.000	-.475	.000	.000
	6	18.6	.000	.000	.862	.000	.000	-.508
NC	1	3.08	.000	.510	.000	.000	.860	.000
	2	3.84	.462	.000	.032	.885	.000	.058
	3	5.52	-.140	.000	.463	-.269	.000	.833
	4	9.24	.000	.854	.000	.000	-.520	.000
	5	13.2	.878	.000	.076	-.470	.000	-.046
	6	17.6	-.303	.000	.809	.171	.000	-.473
SC	1	2.84	.000	.510	.000	.000	.860	.000
	2	3.57	.463	.000	.000	.887	.000	.000
	3	5.13	.000	.000	.485	.000	.000	.874
	4	8.55	.000	.855	.000	.000	-.518	.000
	5	12.3	.882	.000	.000	-.471	.000	.000
	6	16.3	.000	.000	.865	.000	.000	-.502

Table 8 Residuals for the updated  $\mathcal{M}_{8(10)}$  model

Mode	BC configuration			NC configuration			SC configuration		
	$\Delta f_i/f_{ei}$ (%)	MAC <sub>ii</sub>	$f_{ob,i}$ (%)	$\Delta f_i/f_{ei}$ (%)	MAC <sub>ii</sub>	$f_{ob,i}$ (%)	$\Delta f_i/f_{ei}$ (%)	MAC <sub>ii</sub>	$f_{ob,i}$ (%)
1	0.21	1.000	0.24	-0.03	1.000	0.10	-0.22	1.000	0.24
2	0.21	1.000	0.29	-0.24	1.000	0.30	-0.01	1.000	0.19
3	-0.26	0.991	0.99	0.24	0.998	0.47	0.36	0.999	0.47
5	-0.74	1.000	0.75	1.65	0.991	1.89	-0.90	1.000	0.90
6	-0.55	0.991	1.08	-0.27	0.995	0.76	0.61	0.995	0.94

For  $N_u > 10$  the updating problem no longer admits a unique solution. As long as all four mass parameters are included in the updating set,  $\infty^1$  optimal solutions exist for  $N_u = 11$  and  $\infty^2$  for  $N_u = 12$ .

In fact, if more than six stiffness parameters are simultaneously updated the inverse problem becomes under-determined. This can be analytically explained by looking at the structure of the stiffness matrix  $\mathbf{K}$  (Fig. 9). The latter is formed by assembling the  $2 \times 2$  sub-matrices  $\mathbf{K}_x$  and  $\mathbf{K}_y$  of the planar frames along the  $x$  and  $y$  directions. Because of symmetry, these matrices consist of only three independent coefficients each. Therefore, once the optimal  $\mathbf{K}_x$  and  $\mathbf{K}_y$  are found which make  $f_{ob}$  minimum (the inverse problems  $\mathbf{K}_x = g_{x2}^{-1}(f_{ob})$  and  $\mathbf{K}_y = g_{y2}^{-1}(f_{ob})$  are redundant and well conditioned),  $\infty^1$  combinations of the 4 stiffness parameters in the  $x$  direction exist which exactly

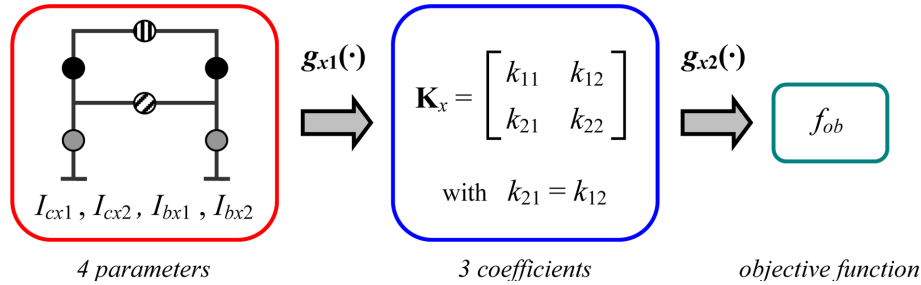


Fig. 9 Non-uniqueness of the solution when four stiffness parameters are assumed as updating variables in the same (e.g.,  $x$ ) direction

Table 9 A sample of the  $\infty^2$  solutions obtained varying the constraints on the 12 parameters

$p_7 / p_5 = p_8 / p_6$ (constraints)	$p_1$ ( $I_{cx1}$ )	$p_2$ ( $I_{cy1}$ )	$p_3$ ( $I_{cx2}$ )	$p_4$ ( $I_{cy2}$ )	$p_5$ ( $I_{bx1}$ )	$p_6$ ( $I_{by1}$ )	$p_7$ ( $I_{bx2}$ )	$p_8$ ( $I_{by2}$ )	d (%)
1/100	.539	.690	3.44	3.55	2.69	2.51	.027	.025	122
1/10	.549	.704	2.73	2.30	2.29	1.92	.229	.192	47.2
1/5	.560	.715	2.20	1.70	1.99	1.63	.399	.327	26.5
1/2	.589	.731	1.41	1.15	1.54	1.37	.771	.685	35.0
2	.646	.743	.728	.862	1.14	1.23	2.28	2.46	71.7
5	.665	.746	.600	.809	1.06	1.21	5.32	6.03	135
10	.672	.747	.562	.792	1.04	1.20	10.4	12.0	226
100	.679	.748	.529	.776	1.02	1.19	102	119	4064

reproduce  $\mathbf{K}_x$ , and the same holds for  $\mathbf{K}_y$  in the  $y$  direction (the inverse problems  $g_{x1}^{-1}(\mathbf{K}_x)$  and  $g_{y1}^{-1}(\mathbf{K}_y)$  are once under-determined). As a consequence, six stiffness parameters (three along  $x$  and three along  $y$ ) uniquely determine  $\mathbf{K}$  and consequently  $f_{ob}$ .

Obviously, the  $\infty^2$  optimal solutions corresponding to assuming  $N_u = 12$  ( $\mathbf{p}_u = \mathbf{p}$ ) or, equivalently, to removing all constraints from the potential updating parameters ( $\mathbf{p}_c = \mathbf{0}$ ) are indistinguishable in terms of the objective function but might be very distant in the search space. One sample from such infinity is model  $\mathcal{M}_{8(10)}$  itself, whose mass properties, modal properties and objective function are identical to those of any other of the  $\infty^2$  solutions.

Table 9 reports a small further sample from that infinity, obtained by imposing two arbitrary constraints (one in each direction) to the eight stiffness parameters included in  $\mathbf{p}$ . Each line corresponds to a different pair of constraints (i.e., to a further model of the multi-model parameterization approach) obtained varying the ratio of the stiffness of upper beams to the stiffness of lower beams from 1/100 to 100. Columns referring to mass parameters and to the objective function are omitted, since identical to those obtained for model  $\mathcal{M}_{8(10)}$ . Once again, the last column represents the distance from  $\mathcal{M}_{8(10)}$  in the search space.

Table 9 reveals the relationship existing, within the subspace of the  $\infty^2$  optimal solutions, among the four stiffness parameters in each direction. As the beam stiffness ratio decreases, the stiffness of lower beams increases whereas that of upper beams very rapidly decreases; to compensate such variations (in order for  $\mathbf{K}$  to keep unchanged), the stiffness of upper columns increases whereas that

of lower columns very slowly decreases. As the beam stiffness ratio increases, reversed trends are observed. The extent to which each parameter varies in Table 9 is an (inverse) measure of the sensitivity of the solution to that parameter or, equivalently, of the robustness of its calibration. So, maximum confidence should be attributed to the updated stiffness of lower columns, minimum confidence to the updated stiffness of upper beams. Therefore, the most reasonable way to impose the *a priori* constraint necessary to avoid under-determinacy seems the assumption, in agreement with visual inspection and design drawings, of a unitary beam stiffness ratio. This is the very assumption at the base of model  $\mathcal{M}_{8(10)}$ , which can finally be regarded as the most plausible of the  $\infty^2$  optimal solutions of the inverse problem.

### 5.3 Discussion of the results

Applied to the model updating of the benchmark case study, the multi-model approach has highlighted important features of the inverse problem, which can be summarized as follows.

The FE model structure depends on a total of  $N_p = 12$  parameters, four governing  $\mathbf{M}$  and eight governing  $\mathbf{K}$ . Once the objective function is defined according to Eq. (1), data collected through a perturbed boundary condition testing are sufficient (and even redundant) to estimate the four mass parameters and six out of eight stiffness parameters. Two stiffness parameters remain indeterminate.

In under-determined problems, the unique solution at a minimum distance from the initial parameters of the baseline model (“minimum norm solution”) is sometimes desired, and obtained by means of regularization techniques. In the present case a multi-model parameterization is applied instead, where alternative solutions are presented to the analyst for an *a posteriori* plausibility verdict.

Models characterized by few updating parameters, although better conditioned, are likely to contain larger errors. Through enlarging the updating set, errors tend to be increasingly corrected and the objective function is progressively reduced. The multi-model approach tracks this trend, comparing alternative parameterizations and rejecting unreliable ones. In the present case study, a single-model approach, whatever the parameterization adopted, because of the small values taken by the objective function in nearly all cases, would have given the false impression of having achieved a successful calibration.

In this multi-model search for the best parameterization, the objective function gets its minimum for any of the  $\infty^2$  optimal solutions obtained through arbitrarily assigning two out of eight stiffness parameters. Interestingly this minimum, although very small, is larger than zero, as the combined effect of data redundancy and presence of error in the measurement/processing chain and in the model structure. The  $\infty^2$  optimal solutions are indistinguishable in terms of the objective function but may significantly deviate from each other in the search domain. A careful examination of few samples indicates that parameters governing beam stiffness are less reliable than parameters governing column stiffness. Based on engineering insight, the most plausible solution among the infinite potential candidates is finally identified as the one which makes the two less sensible parameters, i.e., the stiffness of respectively upper and lower beams, equal to each other. A unique solution is thus obtained, by chance coinciding with model  $\mathcal{M}_{8(10)}$ .

Model  $\mathcal{M}_{8(10)}$  appears therefore the most plausible of the  $\infty^2$  10-parameters models. It could be argued that this model, due to the large number of updating parameters, may suffer from poor conditioning if compared to smaller updating sets. With this in mind, if the whole population of multiple models is re-examined it will be found that model  $\mathcal{M}_{7(8)}$  too seems an excellent candidate,

only a little inferior to  $\mathcal{M}_{8(10)}$  in terms of the objective function but comparable or even preferable for its physical significance, because it anchors the stiffness of the upper columns to its nominal value. Actually, it can be concluded that both models  $\mathcal{M}_{7(8)}$  and  $\mathcal{M}_{8(10)}$ , close to each other in the parameter domain, possess a sound physical meaning and are very reasonable candidates for modelling the benchmark structure.

Two interesting confirmations of these conclusions deserve mentioning.

The first one is the compatibility of both models with the explained phenomenon of braces dynamic interaction. The fourth natural frequency of the model without braces is located in the middle between the two identified frequencies of modes 4a and 4b, and the small modal mass of the fourth mode in the updated model justifies the significance of such interaction.

The second one is the consistent floor sagging estimation achievable using the two best candidate models. To this purpose, the thickness of the concrete slab at the  $i$ -th floor level may be intended not as a constant value but as a 4th order polynomial function of the in-plan coordinates  $x$  and  $y$

$$t_i(x, y) = t_{oi} + s_i(1 - (2x/L_x)^2)(1 - (2y/L_y)^2) \quad (2)$$

where  $L_x$  and  $L_y$  are the slab in-plan dimensions,  $t_{oi}$  is the uniform slab thickness,  $s_i$  is the mid-span slab deflection due to the sagging effect occurred during concrete casting. Accordingly, the slab mass  $m_i$  and the slab polar inertia  $J_{oi}$  are obtained respectively as

$$m_i = \int_A \rho_c t_i(x, y) dA = \rho_c L_x L_y (t_o + 4s_i/9) \quad (3)$$

$$J_{oi} = \int_A \rho_c t_i(x, y) (x^2 + y^2) dA = \rho_c L_x L_y (L_x^2 + L_y^2) (t_o/12 + s_i/45) \quad (4)$$

Taking  $m_i$  and  $J_{oi}$  as provided, for instance, by  $\mathcal{M}_{7(8)}$ , and inverting Eqs. (3) and (4), the uniform thickness and the sagging deflection of the two concrete slabs turn out to be:  $t_{o1} = 6.3$  cm,  $t_{o2} = 6.8$  cm,  $s_1 = 4.2$  cm,  $s_2 = 3.7$  cm. These values sound very reasonable and in good agreement with visual inspection.

## 6. Conclusions

The paper presents an application of ambient-vibration-based model updating to a benchmark building structure, useful to show the significance of modelling errors in structural identification as well as to exemplify some possible countermeasures.

A unique phenomenon of accidental dynamic interaction between main frame and secondary structural elements is first illustrated as an example of errors in the model structure. An *experimental model reduction* is proposed which might be profitably applicable whenever the effects of unmodelled structural elements are known to be confined to a circumscribed region of the experimental data, and this region does not need to be accurately replicated by the model.

A multi-model approach is then presented to deal with errors in model parameters, consisting in the generation and solution of a multitude of models, all sharing the same model structure but differing from each other in terms of the updating set. By enlarging the updating set until reaching non-uniqueness of the solution, an entire population of candidate models is derived which improves

the general understanding of the inverse problem and allows, with the support of engineering insight, an *a posteriori* selection of the most plausible solution(s).

Main conclusions from this study can be summarized as follows:

- Even in the case of seemingly simple systems model-updating is not an easy task and may be biased by errors in the model structure as well as by an improper choice of the updating parameters;
- Unaccounted secondary structural elements may act as a severe misleading factor in system identification; their lightness is not a sufficient condition to neglect them whenever a dynamic interaction with the main structure can not be excluded;
- Spanning alternative modelling assumptions (multi-model parameterization) is an effective strategy to depict to which extent results depend on the arbitrary choice of the updating set, and ultimately to increase calibration robustness;
- Small absolute values of the error function are not a reliable index of successful updating; since small improvements in the error function may correspond to large variations in the domain of physical parameters, every care must be taken to minimize all possible errors inherent in measurement, processing, modelling and optimization;
- Whenever the updating parameters are too many to avoid ill-conditioning or under-determinacy, physical insight is needed; models can only be accepted if sound physical explanation is found; when physical justifications cannot be found models should be rejected; if it is not possible to obtain a unique identification, alternative plausible candidates are identified for subsequent use.

The results of this work have been successfully used in the subsequent phases of the DPC-ReLUIIS 2005-08 Project to simulate the response of the benchmark structure in its controlled configuration.

## References

- Adhikari, S. and Friswell, M.I. (2010), "Distributed parameter model updating using the Karhunen-Loève expansion", *Mech. Syst. Signal Pr.*, **24**, 326-339.
- Altunişik, A.C., Bayraktar, A., Sevim, B., Kartal, M.E. and Adanur, S. (2010), "Finite element model updating of an arch type steel laboratory bridge model using semi-rigid connection", *Steel Compos. Struct.*, **10**(6), 543-563.
- Aoki, T. and Sabia, D. (2005), "Structural identification and seismic performance of brick chimneys, Tokoname, Japan", *Struct. Eng. Mech.*, **21**, 553-570.
- Bayraktar, A., Altunişik, A.C., Sevim, B. and Turker, T. (2010), "Finite element model updating of K m rhan highway bridge based on experimental measurements", *Smart Struct. Syst.*, **6**(4), 373-388.
- Bonato, P., Ceravolo, R., De Stefano, A. and Molinari, F. (2000), "Use of cross time-frequency estimators for the structural identification in non-stationary conditions and under unknown excitation", *J. Sound Vib.*, **237**, 775-791.
- Brincker, R., Zhang, L. and Andersen, P. (2001), "Modal identification of output-only systems using frequency domain decomposition", *Smart Mater. Struct.*, **10**, 441-445.
- Cheung, S.H. and Beck, J.L. (2009), "Bayesian model updating using hybrid Monte Carlo simulation with application to structural dynamic models with many uncertain parameters", *J. Eng. Mech.*, **135**(4), 243-255.
- Den Hartog, J.P. (1956), *Mechanical Vibrations*, 4th Edition, McGraw-Hill, New York.
- Friswell, M.I. and Mottershead, J.E. (1995), *Finite Element Model Updating in Structural Dynamics*, Kluwer Academic Press, Dordrecht, The Netherlands.
- Giraldo, D.F., Song, W., Dyke, S.J. and Caicedo, J.M. (2009), "Modal identification through ambient vibration: Comparative study", *J. Eng. Mech.*, **135**(8), 759-770.

- Govers, Y. and Link, M. (2010), "Stochastic model updating – Covariance matrix adjustment from uncertain experimental modal data", *Mech. Syst. Signal Pr.*, **24**, 696-706.
- Juang, J.N. and Pappa, R.S. (1984), "An eigensystem realisation algorithm (ERA) for modal parameter identification and modal reduction", *Proceedings of NASA/JPL Workshop on Identification and Control of Flexible Space Structures*.
- Jung, D.S. and Kim, C.Y. (2009), "FE model updating based on hybrid genetic algorithm and its verification on numerical bridge model", *Struct. Eng. Mech.*, **32**(5), 667-683.
- Kim, G.H. and Park, Y.S. (2008), "An automated parameter selection procedure for finite-element model updating and its applications", *J. Sound Vib.*, **309**, 778-793.
- Levin, G.R.I. and Lieven, N.A.J. (1998), "Dynamic finite element model updating using simulated annealing and genetic algorithms", *Mech. Syst. Signal Pr.*, **12**(1), 91-120.
- Li, X.Y. and Law, S.S. (2010), "Adaptive Tikhonov regularization for damage detection based on nonlinear model updating", *Mech. Syst. Signal Pr.*, **24**, 1646-1664.
- Maia, N.M.M. and Silva, J.M.M. (1997), *Theoretical and Experimental Modal Analysis*, Research Studies Press Ltd., Somerset.
- McFarland, J. and Mahadevan, S. (2008), "Error and variability characterization in structural dynamics modelling", *Comput. Meth. Appl. M.*, **197**, 2621-2631.
- Mottershead, J.E., Link, M. and Friswell, M.I. (2011), "The sensitivity method in finite element model updating: A tutorial", *Mech. Syst. Signal Pr.*, **25**, 2275-2296.
- Mthembu, L., Marwala, T., Friswell, M.I. and Adhikari, S. (2011), "Model selection in finite element model updating using the Bayesian evidence statistic", *Mech. Syst. Signal Pr.*, **25**, 2399-2412.
- Nalitolela, N.G., Penny, J.E.T. and Friswell, M.I. (1992), "A mass or stiffness addition technique for structural parameter updating", *Int. J. Analyt. Exp. Mod. Anal.*, **7**(3), 157-168.
- Peeters, B. and Ventura, C.E. (2003), "Comparative study of modal analysis techniques for bridge dynamic characteristics", *Mech. Syst. Signal Pr.*, **17**(5), 965-988.
- Perera, R. and Ruiz, A. (2008), "A multistage FE updating procedure for damage identification in large-scale structures based on multiobjective evolutionary optimization", *Mech. Syst. Signal Pr.*, **22**, 970-991.
- Raphael, B. and Smith, I.F.C. (2003), "A direct stochastic algorithm for global search", *Appl. Math. Comput.*, **146**(2-3), 729-758.
- Robert-Nicoud, Y., Raphael, B., Burdet, O. and Smith, I.F.C. (2005), "Model identification of bridges using measurement data", *Comput.-Aided Civ. Inf.*, **20**, 118-131.
- Saitta, A., Raphael, B. and Smith I.F.C. (2005), "Data mining techniques for improving the reliability of system identification", *Adv. Eng. Inform.*, **19**, 289-298.
- Sanayei, M., Wadia-Fascetti, S., Arya, B. and Santini, E.M. (2001), "Significance of modelling error in structural parameter estimation", *Comput.-Aided Civ. Inf.*, **16**, 12-27.
- Yan, G., Duan, Z. and Ou, J. (2010), "Damage detection for beam structures using an angle-between-string-and-horizon flexibility matrix", *Struct. Eng. Mech.*, **36**(5), 643-667.
- Yu, E. and Chung, L. (2012), "Seismic damage detection of a reinforced concrete structure by finite element model updating", *Smart Struct. Syst.*, **9**(3), 253-271.
- Zapico-Valle, J.L., Alonso-Cambor, R., Gonzalez-Martinez, M.P. and Garcia-Dieguez, M. (2010), "A new method for finite element model updating in structural dynamics", *Mech. Syst. Signal Pr.*, **24**, 2137-2159.
- Zarate, B.A. and Caicedo, J.M. (2008), "Finite element model updating: Multiple alternatives", *Eng. Struct.*, **30**, 3724-3730.